ACS SyntheticBiology

pubs.acs.org/synthbio

Research Article

New Insight into Plasmid-Driven T7 RNA Polymerase in *Escherichia coli* and Use as a Genetic Amplifier for a Biosensor

Shih-I Tan and I-Son Ng*

Cite This: *ACS Synth. Biol.* 2020, 9, 613–622

Read Online

ACCESS | Metrics & More | Article Recommendations | Supporting Information

ABSTRACT: T7 RNA polymerase (T7RNAP) and T7 promoter are powerful genetic components, thus a plasmid-driven T7 (PDT7) genetic circuit could be broadly applied for synthetic biology. However, the limited knowledge of the toxicity and instability of such a system still restricts its application. Herein, we constructed 16 constitutive genetic circuits of PDT7 and investigated the orthogonal effects in toxicity and instability. The T7 toxicity was elucidated from the construction processes and cell growth characterization, showing the importance of optimal orthogonality for PDT7. Besides, a protein analysis was performed to validate how the T7 system affected cell metabolism and led to the instability. The application of constitutive PDT7 in functional protein expressions, including carbonic anhydrase, lysine decarboxylase, and 5-ALA synthetase was demonstrated. Furthermore, PDT7 working as a genetic amplifier had been designed for *E. coli* cell-based biosensors, which illustrated the opportunities in the future of PDT7 used in synthetic biology.

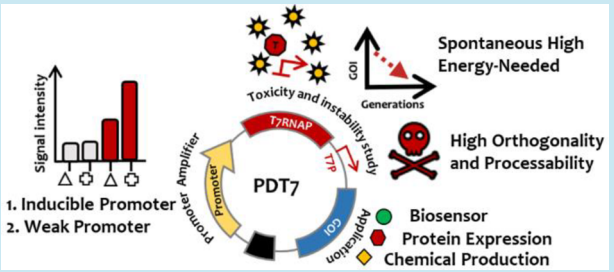

KEYWORDS: *synthetic biology, T7 RNA polymerase, plasmid-driven T7, genetic amplifier, cell-based biosensor*

Programming cellular behavior toward wide-ranging applications, such as biosensing, digital, and analog computation, cell state memory, biosynthesis of valuable chemicals, and bioremediation is the central dogma of synthetic biology.[1,2] Recently, it has migrated from reconstructing model organisms to other robust chassis that possesses better tolerance to the desired metabolites or survives more readily in harsh conditions.[3,4] Therefore, it is more applicable and straightforward to develop a universal toolkit for a large numbers of noncanonical chassis.

T7 RNA polymerase (T7RNAP) was isolated from the bacteriophage T7 and has been studied since 1970[5] in the areas of optimal production,[6,7] protein structure,[8,9] biochemical aspects, and transcriptional mechanism.[10,11] Comprehensive studies have proven that T7RNAP is a powerful transcription system for host-independent expression, owing to the functional single-subunit enzyme with high processivity, high specificity for the T7 promoter, and no need of any auxiliary transcription factors.[12] The widely known application of T7RNAP is the pET system in *E. coli* for protein overexpression, for which a lysogenic DE3 host containing one copy of the T7 RNAP gene under the control of lacUV5 promoter in the chromosome and a cognate plasmid containing a T7 promoter are used.[6] Notably, a single copy of T7RNAP is sufficient to induce targeted protein in high-level expression, while excessive T7RNAP causes a lethal effect on the cell.[7] Therefore, several noncanonical organisms were equipped with the chromosome-integrated T7RNAP (CIT7), but the technology was still restricted to limited genomic information and less of available genetic editing tools.[12] Besides, it is time-consuming and labor-intensive to finetune and optimize the efficiency of T7RNAP expression in CIT7. Alternatively, the plasmid-driven T7RNAP (PDT7), in which T7RNAP is expressed by a plasmid, has been developed and widely applied in synthetic biology as controllers,[13] logic gates,[14] resource allocators,[15] and orthogonal systems recently.[16]

The PDT7 system possesses more applications than CIT7 because the plasmid is more conducive to manipulate. For example, two PDT7 systems called "Universal Bacterial Expression Resource (UBER)" and "Host-Independent T7 Expression System (HITES)" were established and utilized in Gram-positive cells (i.e., *Corynebacterium glutamicum* and *Bacillus subtilis*) and Gram-negative bacteria (i.e., *Pseudomonas putida*, *Sinorhizobium*, and *Tatumella morbirosei*).[17,18] Two platforms are regulated under an inducible system to express the T7RNAP, but it is not the best strategy to engineer a robust industrial strain as it requires an inducer at optimal condition. Although the unstable expression of PDT7 occurring in HITES has been solved by decreasing T7RNAP expression, how T7RNAP affects cell behavior and causes instability remains unknown.[18] On the other hand, particularly

Received: November 19, 2019
Published: March 6, 2020

https://dx.doi.org/10.1021/acssynbio.9b00466
ACS Synth. Biol. 2020, 9, 613–622

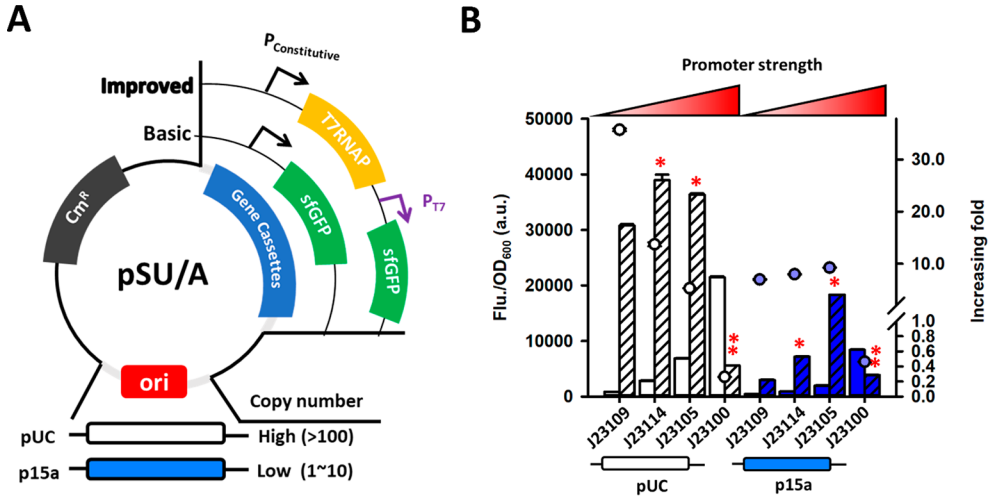

Figure 1. Development of constitutive plasmid-driven T7 system. (A) Design of genetic circuits. Basic cassettes contain a constitutively expressed sfGFP. Improved cassettes contained a constitutively expressed T7RNAP and a T7-sfGFP. (B) Fluorescence intensity of 16 constructs. The white or blue color indicates high-copy-number ori (pUC) or low-copy-number ori (p15a). The bars with or without lines indicate the improved or basic cassette, respectively. The bar shows the specific fluorescence intensity (Flu/OD_{600}), and the circle symbol shows the increasing fold of sfGFP between the basic and improved cassettes. *mutation of the T7 promoter; **frame shift on the T7RNAP. Error bars represent the s.d. (standard deviation) of three independent experiments (n = 3).

in PDT7, T7RNAP is typically split in cellular engineering, which has been reported to reduce the lethal effect and biological stress caused by excess T7RNAP from the multicopy plasmid,[7,19−22] but the reason why splitting T7RNAP or lower T7RNAP expression could reduce the negative effect is still unknown. On the other hand, similar to using CIT7, construction of splitting T7RNAP is time-consuming and labor-intensive, thus the full-length T7RNAP is also a promising and convenient option in application.

As aforementioned, inducible PDT7 is achievable in cellular engineering of nonmodel organisms, but no constitutive PDT7 has been reported. In this study, we first constructed 16 different combinations of constitutive PDT7 and provided a platform to straightforwardly quantify the effectiveness of PDT7 by superfolder GFP (sfGFP). During the construction of constitutive PDT7, the toxicity of the T7 system was elucidated. Furthermore, according to biological central dogma, we analyzed plasmid copy numbers by qPCR, transcriptional levels by qRT-PCR, and protein expression by SDS-PAGE to clarify the behavior of cells under regulation by PDT7. In addition, a tandem MS/MS identification of selective proteins was used to decipher the instability of PDT7, which revealed a new mechanism of unstable expression. We also expressed the different enzymes by constitutive PDT7 and characterized the activity. Finally, an amplifier using PDT7 on whole cell biosensing was also exploited.

RESULTS AND DISCUSSIONS

Development of Constitutive PDT7 System in *E. coli*.

Two different gene circuits, defined as the basic and improved cassettes, were used to evaluate protein expression, in which the basic cassette contained a constitutive promoter to express sfGFP while the improved cassette, also called PDT7, contained the same promoter to express T7RNAP and its orthogonal T7-sfGFP cassettes (Figure 1A). All gene circuits expressed sfGFP, which were directly or indirectly controlled by promoters of four different strengths from iGEM (i.e., J23100, J23105, J23114, and J23109, Table S1). Regarding previous reports, the targeted protein could be massively expressed by a few T7RNAPs in the T7 system.[6,7] Therefore, we cloned two cassettes into a plasmid with a low copy number (i.e., p15a origin of replication, pSA plasmid). The order of sfGFP intensity matched the order of promoter strength in the basic cassettes (Figure 1B, blue bars). On the other hand, using T7RNAP as the amplifier (i.e., pSA-J23109-PDT7, pSA-J23114-PDT7*, and pSA-J23105-PDT7*) could increase the expression of sfGFP within the PDT7 improved cassette (Figure 1B, blue lined bar), and achieve an average 9-fold increase when compared to that of the basic cassettes (Figure 1B, blue dot). Unexpectedly, under the control of the strongest promoter J23100 in PDT7 improved cassette (pSA-J23100-PDT7**), the sfGFP expression decreased to 40%.

Although the improved cassettes in low copy plasmids had successfully increased the sfGFP expression, the level of Flu/OD was lower than 20 000 and 10 000 for improved and basic circuits, respectively. To overcome this problem, two cassettes were cloned into the plasmid with a high copy number (i.e., pUC origin of replication, pSU plasmid). For the basic cassette, the order of fluorescence intensity was consistent with the order of promoter strength, and the corresponding sfGFP intensity was much higher than that in the low-copy-number plasmid (Figure 1B, white bars). Importantly, sfGFP intensity increased dramatically in the improved cassette (i.e., 35-fold, Figure 1B, white dot) under the J23109 promoter (Figure 1B, white lined bars, pSU-J23109-PDT7). Moreover, further enhancement of the promoter strength in the improved cassettes (i.e., pSU-J23114-PDT7* and pSU-J23105-PDT7*) could further increase the sfGFP expression when compared to using J23109 as promoter (pSU-J23109-PDT7). Conversely, using the strongest promoter J23100 to drive the T7RNAP showed a decrease of the sfGFP expression, which was consistent to the outcome in the low-copy plasmid. The negative results of PDT7 driven by J23100 (pSU-J23100-PDT7**) is supposedly due to a toxic effect and will be discussed in the next section. This is the first-time the constitutive PDT7 system was developed for *E. coli*. The higher fluorescence intensity is obtained from improved cassettes in high-copy plasmids, and is similar to that obtained by

https://dx.doi.org/10.1021/acssynbio.9b00466
ACS Synth. Biol. 2020, 9, 613−622

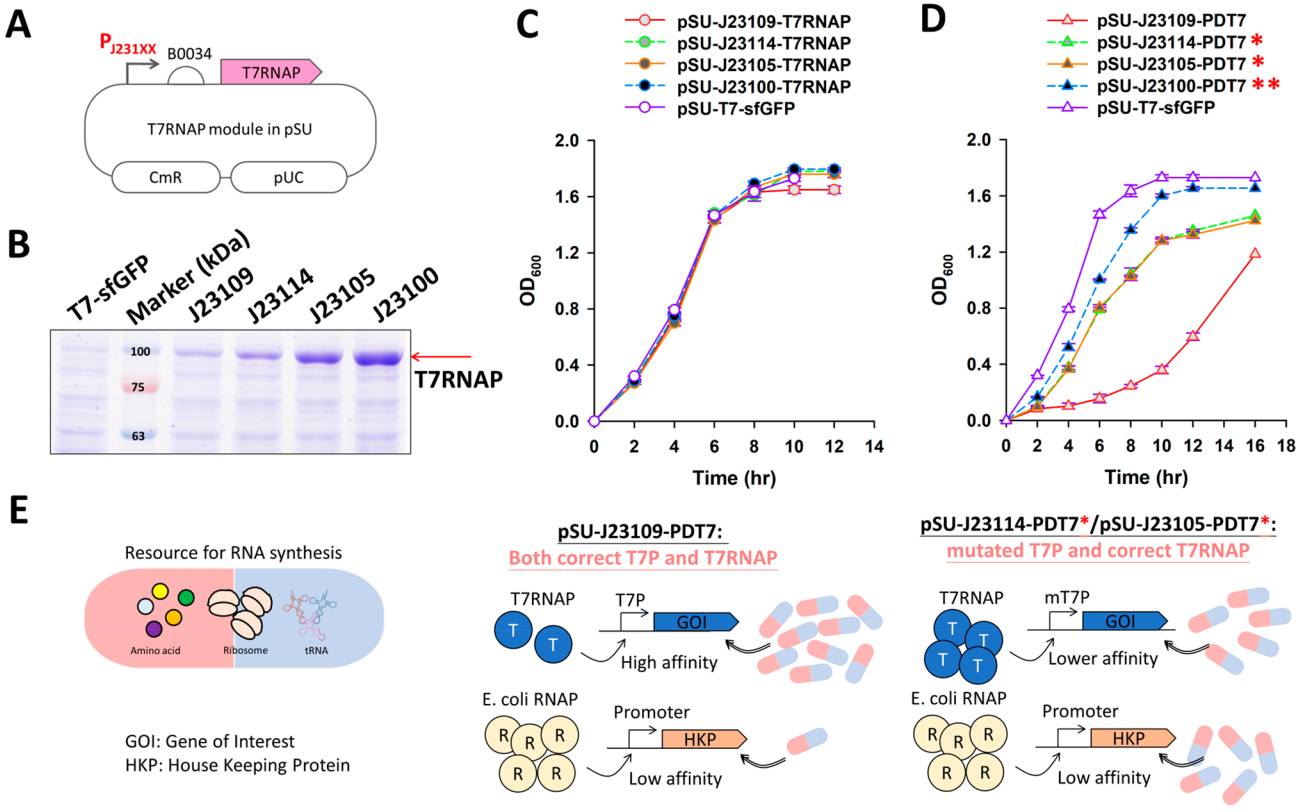

Figure 2. Toxicity study using constitutive PDT7. (A) Construction map of pSU-J231XX-T7RNAP. (B) SDS-PAGE results of T7RNAP under different J-series promoters. The arrow was used to indicate the T7RNAP expression band. (C) Growth curve of DH5α harboring the pSU-J231XX-T7RNAP. The purple circle is the DH5α harboring pSU-T7-sfGFP as the control. The red, green, orange, and blue circle, respectively, represent the DH5α harboring the pSU-J23109-T7RNAP, pSU-J23114-T7RNAP, pSU-J23105-T7RNAP, and pSU-J23100-T7RNAP. (D) Growth curve of DH5α harboring the pSU-J231XX-PDT7. The purple triangle is the DH5α harboring pSU-T7-sfGFP as the control. The red, green, orange, and blue triangle, respectively, represent the DH5α harboring the pSU-J23109-PDT7, pSU-J23114-PDT7*, pSU-J23105-PDT7*, and pSU-J23100-PDT7**. Error bars represent the s.d. (standard deviation) of three independent experiments (n = 3). (E) Proposed mechanism to describe the toxicity of T7RNAP with T7 promoter. The resource of RNA synthesis represented in a capsule and requires the amino acid, ribosome, and tRNA. The competition between the T7 system and house keeping protein (HKP) expression is the major reason for T7RNAP toxicity. *mutation of the T7 promoter; **frame shift on the T7RNAP.

increasing the T7 cassette copy from replication ori of pBR322 to RSF that possesses 300−500 copies per cell increases the protein expression.[23]

Constitutive PDT7 Proves the Toxicity Caused by Orthogonal T7RNAP and T7 Promoter. To ascertain the effectiveness of PDT7, we sequenced all constructions with the J-series promoters, T7RNAP and T7 promoter. The results showed a single T missing on the 14th nucleotide of T7 promoter in the pSU-J23114-PDT7* and pSU-J23105-PDT7*, and the frameshift in T7RNAP in pSU-J23100-PDT7** (Figure S1 and Table S2), which occurred because the construction flow by PCR to amplify the T7RNAP and T7-sfGFP cassette introduced mismatched nucleotides (Figure S2). Therefore, the reconstruction of the plasmids was changed to digestion to prevent PCR-induced errors. But we failed to construct it, indicating the toxicity of the T7 system caused cell burden and collapsed the construction.

We hypothesized that the toxicity of the T7 system was not due to the T7RANP expression but the orthogonality of the T7 system instead. Thus, we constructed the basic part with T7RNAP (Figure 2A) and measured protein expression (Figure 2B) as well as cell growth (Figure 2C). The expression of T7RNAP indicated by the arrow at 99 kDa rose as the promoter strength increased, while we used T7-sfGFP as a control to show no T7RNAP would be expressed (Figure 2B). As similar cell growth was observed from the strains with different expression levels of T7RNAP (Figure 2C), our first hypothesis was proven.

Next, we examined the cell growth of constructed PDT7, which exhibited a serious growth retardation for pSU-J23109-PDT7, and a slight growth retardation for pSU-J23114-PDT7* and pSU-J23105-PDT7* (Figure 2D). The results displayed that the correct sequence of T7RNAP and T7 promoter in the pSU-J23109-PDT7 would severely retard cell growth due to the high orthogonality. On contrast, the lower affinity of the mutated T7 promoter and correct T7RNAP escaped the growth retardation (i.e., pSU-J23114-PDT7* and pSU-J23105-PDT7*). As a frame shift explored in the pSU-J23100-PDT7** system that was without orthogonality, the cell growth showed no significant difference compared to the DH5α harboring pSU-T7-sfGFP.

Consequently, a mechanism was supposed to illustrate the toxicity of the T7 system. The RNA synthesis required the amino-acids, ribosome, and tRNA (tRNA) (Figure 2E, left). In the correct T7 promoter and T7RNAP clones (i.e., pSU-J23109-PDT7), due to the competition of RNA synthesis resource between the higher affinity T7 system and relatively lower affinity house-keeping protein (HKP) expression at the

https://dx.doi.org/10.1021/acssynbio.9b00466
ACS Synth. Biol. 2020, 9, 613−622

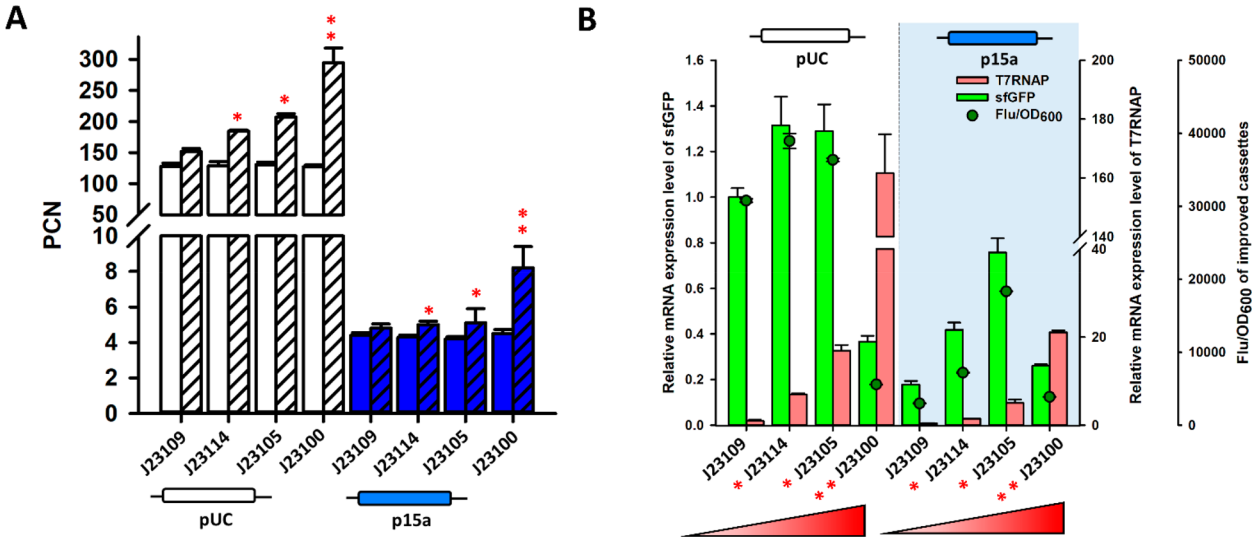

Figure 3. Cell behavior analysis of PDT7. (A) Copy number analysis. The bars with or without slope lines indicate the improved gene cassette or basic cassette, respectively. The white or red color indicated that the high-copy-number ori (pUC) or low-copy-number ori (p15a) was used, respectively. (B) Transcription analysis of improved cassettes by qRT-PCR. Green or pink bars indicate the relative mRNA expression of sfGFP and T7RNAP, respectively. The reference sample was PDT7 controlled by J23109 in a high-copy-number plasmid. The circles indicate the corresponding specific fluorescence intensity. Error bars represent the s.d. (standard deviation) of three independent experiments (n = 3).

early stage of cell growth, it acquired a few resources for HKP synthesis (Figure 2E, middle), resulting in the serious retardation of cell growth. For the pSU-J23105-PDT7* and pSU-J23114-PDT7* containing the mutated T7 promoter and correct T7RNAP, even though there is a higher expression level of T7RNAP, the mutated T7 promoter afforded low affinity to each other; thus, the competition between the T7 system and HKP synthesis was weak (Figure 2E, right), leading to a slight cell growth delay. The failed constructions of correct pSU-J23114-PDT7, pSU-J23105-PDT7, and pSU-J23100-PDT7 were due to the strongly aggressive competition; thus, mutation or cell death was observed during the construction.

The constitutive PDT7 is a simplified system and provides a straightforward symptom toward the T7RNAP toxicity compared to the inducible system. In a previous report, T7RNAP toxicity in an "inducible" system due to the T7RNAP expression even without the T7 promoter had been addressed.[13] However, as shown by our results, constitutive T7RNAP overexpression did not confer the cell burden. On the other hand, although T7RNAP toxicity has been observed to be more serious as the T7 promoter presented,[13] how it affects the cell growth is still not reported in the literature. Herein, we propose a competition model between the T7 system and HKP synthesis to describe how T7 orthogonality affects cell growth and the plasmid construction. For direct evidence to support our proposed model, the cell harboring pSU-J23109-PDT7 at the early lag phase (i.e., 8 h) was collected and analyzed by SDS-PAGE to observe the difference of protein expression, especially for HKP. As shown in Figure S3, very less protein accumulated when compared to that in the DH5α at the same time, which indicated the toxicity of T7 system. Furthermore, the proposed mechanism is also supported by the existing strategy to reduce T7RNAP toxicity from the orthogonality, including mutation on T7RNAP and T7 promoter,[13,24] splitting the T7RNAP,[19−22] and reduction of T7RNAP production.[13,18]

Central Dogma Analysis of Constitutive PDT7 in *E. coli*. To determine the critical factors that affect PDT7, a checking process was carried out to reveal the performance of the plasmid copy number (PCN), transcription (TX), and translation (TL) in constitutive PDT7. The PCN was reasonably similar to the previously reports but increased from 150 to 300 in the high-copy-number plasmid (i.e., pUC ori), and from 5 to 9 in the low-copy-number plasmid (i.e., p15a ori) as shown in Figure 3A. The average PCN of PDT7 was slightly higher than that in the basic cassette. The PCN is not restricted to the specific value; instead, it may change within a moderate range depending on the element exited in the plasmid and the culturing environment.[25]

By qRT-PCR analysis, the transcription of T7RNAP corresponded to the promoter strength that the relative mRNA of T7RNAP had reached, 160 by the J23100 promoter (Figure 3B, pink bar). The transcription of sfGFP (Figure 3B, green bar) was also consistent with the fluorescence intensity (Figure 3B green dot). However, sfGFP levels critically trended down under the strongest promoter J23100 in both p15a and pUC plasmids. The protein translation was confirmed by SDS-PAGE (Figure S4), in which sfGFP expression at 27.1 kDa was matched to sfGFP transcription and fluorescence intensity (Figure S4, sfGFP). However, T7RNAP expression at 99.1 kDa was inconsistent with transcription under the strongest promoter, J23100 (Figure S4, T7RNAP). Therefore, the decreased fluorescence intensity of the PDT7 improved cassette under J23100 promoter was attributed to the decreased expression of T7RNAP. From the translational sequence results in Figure S5, the T7RNAP in pSU-J23100-PDT7** would not be expressed in its functional form; instead, a calculated 3.2 kDa peptide may be produced but it would not be observed by SDS-PAGE due to the difficulty of peptide production in *E. coli*. As a conclusion, the PCN normally exists while the orthogonal T7RNAP and T7 promoter is the key of whole system and thus dominates the translational levels of T7RNAP and the downstream gene (i.e., sfGFP).

Protein Analysis Provides New Insight into the Stability of the PDT7 System. One of the major concerns

https://dx.doi.org/10.1021/acssynbio.9b00466
ACS Synth. Biol. 2020, 9, 613−622

of plasmid-based expression is stability. As shown in Figure 4A, the relative fluorescence intensity of PDT7 under the J23109,

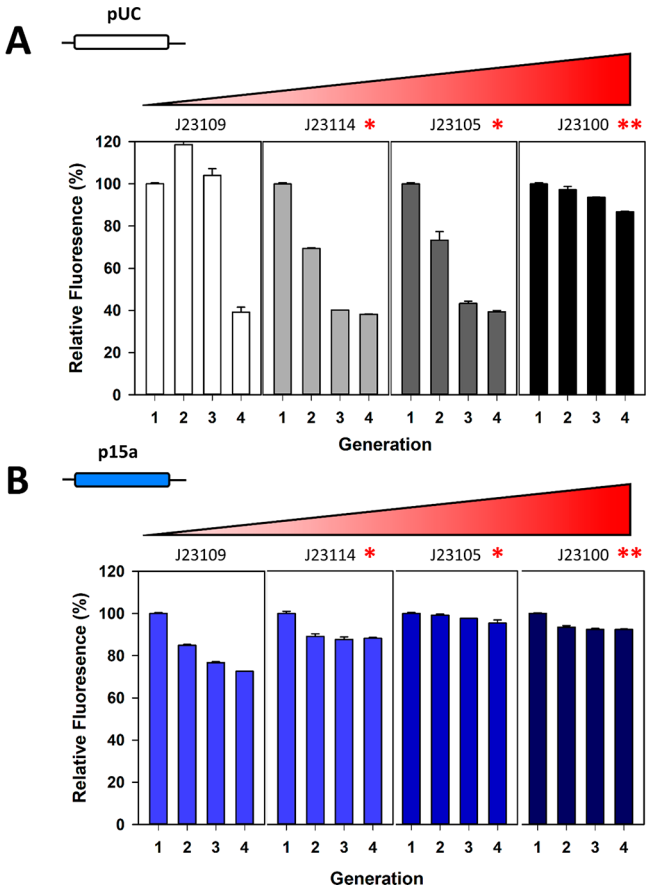

Figure 4. Stability test of PDT7 in high-copy plasmid and low-copy plasmid within four generations. (A) High-copy ori pUC plasmid. (B) Low-copy ori p15a plasmid. Error bars represent the s.d. (standard deviation) of three independent experiments (n = 3). *mutation of the T7 promoter; **frame shift on the T7RNAP.

J23114*, and J23105* promoters in high-copy plasmid decreased to 38% at the fourth generation in high-copy-number PDT7, but it did not change in the low copy plasmid (Figure 4B). The fluorescence intensity in pSU-J23100-PDT7** over four generations is stable because a frame shift in T7RNAP occurs; thus, there is no orthogonal effect of the T7RNAP and T7 promoter. For the PDT7 with the highest performance (i.e., pSU-J23114-PDT7*), the relative fluorescence decreased to 70% and 40% in intensity at the second generation and third generation, respectively. The decrease in fluorescence intensity in pSU-J23109-PDT7 and pSU-J23105-PDT7* was similar to that of pSU-J23114-PDT7*; therefore, we speculated that the stress and toxicity were caused by expression of T7RNAP with its orthogonal T7 cassette, even with a single mutation or not, to result in unstable PDT7 over the generations.

To decipher the assumption more clearly, we selected the J23114-improved circuit in the high-copy-number plasmids (i.e., pSU-J23114-PDT7*) for further analysis. The results showed that the PCN remained at the same level over generations (Figure 5A), indicating that the fluorescence decrease was not attributable to plasmid loss. Next, SDS-PAGE was carried out to analyze the protein pattern and expression over the generation (Figure 5B). By analysis from ImageLab software, three bands (i.e., T7, U, and D) slightly increased (Figure S6A to S6C), and one major band (i.e., G) was significantly decreased (Figure S6D). The four target bands were further analyzed by liquid chromatography and tandem mass spectrometry (LC−MS/MS) to acchieve *de novo* sequences, and results were run through the MASCOT database to identify the proteins. The proteins with higher scores from four target bands were illustrated in Table 1, in which the T7-1 and G band were affirmed to be the T7RNAP and green fluorescence protein, respectively (Table 1). Besides T7RNAP and sfGFP, five predicted proteins were classified in the energy-producing tricarboxylic acid (TCA) cycle (i.e., T7-2 and T7-3) and amino acid metabolism (i.e., U-1, U-2, and D); therefore, we have suggested a mechanism called "Energy-Deficiency-Induced Interference in Amino Acid Metabolism" (Figure 5C). The peptides or incomplete translations were decomposed by peptidase (*pep*N), and the tryptophan and cysteine were further transformed into pyruvate via tryptophanase (*tna*A) and cysteine desulfhydrase (*dcy*D), respectively. Finally, the carbon flux from pyruvate to the TCA was enhanced to accumulate more energy to implement the energy deficiency, which was catalyzed by pyruvate dehydrogenase (*ace*E) and bifunctional aconitate hydratase 2/2-methylisocitrate dehydratase (*acn*B/*acn*A). Actually, the RNA and protein synthesis both are coupling and require energy in *E. coli*, indicating an intensive energy demand in the T7 system. As previous results show in Figure 2D, the retardation of cell growth at the early stage and the reduction of biomass at the stationary phase are caused by the high energy requirement of PDT7 in the high-copy plasmid, thus activating the proteins related to the TCA cycle to support the cell growth.

To overcome the energy deficiency (i.e., ATP and NADH shortage) in PDT7, we added 1, 5, and 10 g/L casamino acid as the extra amino acid to the culture. The biomass increased along with the addition of more casamino acids from first to fourth generation (Figure 5D, right *Y*-axis). Moreover, adding the casamino acids kept the fluorescence intensity higher than that without casamino acid, but it only maintained for two generations and decreased afterward. At the fourth generation, the relative specific fluorescence for 10, 5, 1, and 0 g/L of casamino acids ranked from 53%, 49%, 44%, and 40% (Figure 5D, left *Y*-axis). We also calculate the specific enhancement on casamino acid concentration at the fourth generation, which is 4% for 1 g/L, 1.8% for 5 g/L, and 1.3% for 10 g/L of casamino acids addition (Table S3). The additional casamino acid not only provided the amino acid for recombinant protein production (i.e., sfGFP), but also distributed it for the T7RNAP expression. Thus, it increases the orthogonality and stress in the cell, leading to inefficient energy complementation and decreasing relative specific fluorescence with each generation (Figure 5D).

In fact, the unstable expression levels over the generations are commonly observed in the plasmid-driven expression without the resistance, which is ascribed to the loss of plasmid.[25] In addition, even with antibiotics, unstable expression was also observed, which is suggested by plasmid random inheritance.[26] The CFU analysis of PDT7 showed only two types of colony, indicating random inheritance did not dominate in this system (data not shown). On the other hand, Liang and his co-worker explained that the unstable expression in PDT7 was due to the biological stress of expression of T7 RNAP.[18] Here, we provide a more detailed

https://dx.doi.org/10.1021/acssynbio.9b00466
ACS Synth. Biol. 2020, 9, 613−622

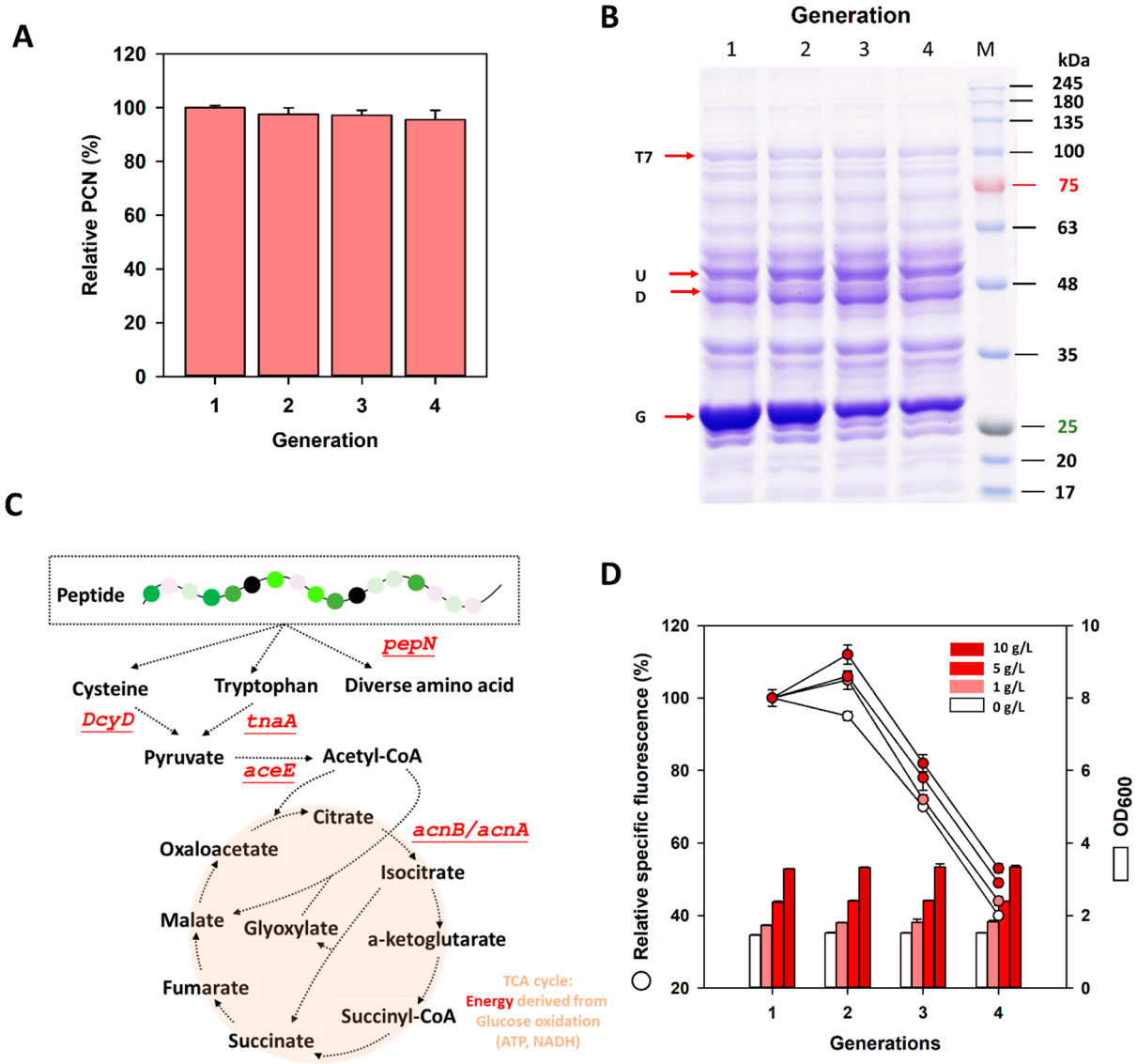

Figure 5. Protein analysis of unstable protein expression in the J23114-driven PDT7 system in a high-copy-number plasmid. (A) Plasmid copy number (PCN) within four generations. (B) SDS-PAGE analysis in which the bands indicated by the red arrows were selected for liquid chromatography tandem mass spectrometry (LC−MS/MS) analysis, and the name is shown near the arrows. (C) Suggested mechanism "Energy-Deficiency Induced Interference of Amino acid Metabolism" for the explanation of unstable expression of PDT7. (D) Effect of the addition of casamino acid for the best PDT7 system, left *Y*-axis indicates the relative specific fluorescence (%) and right *Y*-axis represents the biomass by OD_{600}. Error bars represent the s.d. (standard deviation) of three independent experiments (n = 3).

Table 1. Mascot Protein Analysis of LC−MS/MS Results[a]

no.	protein name	accession no.	score	MW (Da)	pI	coverage (%)
T7-1	DNA-dependent RNA polymerase (*T7RNAP*)	WP_001092355.1	848	98.79	6.77	17
T7-2	pyruvate dehydrogenase (*aceE*)	WP_096147627.1	1029	99.60	5.46	19
T7-3	bifunctional aconitate hydratase 2/2-methylisocitrate dehydratase (*acnB/acnA*)	WP_053901599.1	1295	93.40	5.24	27
U-1	cysteine desulfhydrase (*dcyD*)	KFH77304.1	1021	52.72	5.88	44
U-2	tryptophanase (*tnaA*)	WP_001555276.1	1024	52.74	6.00	44
D	aminopeptidase (*pepN*)	WP_096962388.1	524	46.17	5.73	24
G	superfold green fluorescent protein (sfGFP)	JQ341914.1	313	27.09	5.93	23

[a]Total protein of the best PDT7, in which J23114 was selected to drive the expression of T7RNAP and pUC ori was used, was extracted by high pressure homogenizer for four generations, and analyzed by SDS-PAGE. Three protein bands were selected and named as T7, U, and D.

mechanism of unstable expression in PDT7 caused by Energy-Deficiency-Induced interference in the amino acid metabolism.

Pathway Engineering Using PDT7. For further application, we selected three proteins including carbonic anhydrase from *Helicobacter pylori* (HpCA), lysine decarboxylase from *E. coli* (EcCadA), and aminolevulinic acid synthase from *Rhodobacter sphaeroides* (RsHemA) to express via PDT7 and compared those with the wild type DH5α and that harboring

https://dx.doi.org/10.1021/acssynbio.9b00466
ACS Synth. Biol. 2020, 9, 613−622

the basic cassette. The results indicated that the heterologous protein could be expressed with detectable functions. Carbonic anhydrase catalyzes the hydration of carbon dioxide to the bicarbonate, which has been reported to be highest potential solution toward the green-house effect (Figure S7A). The cell expressing the HpCA from PDT7 used as a whole-cell catalyst for carbon fixation showed 189.7 WAU/mL compared to 73.4 and 105.5 WAU/mL from wild-type DH5α and that harboring the basic cassette, demonstrating a 2.58-fold and 1.80-fold increase (Figure 6, HpCA), respectively. The residual activity

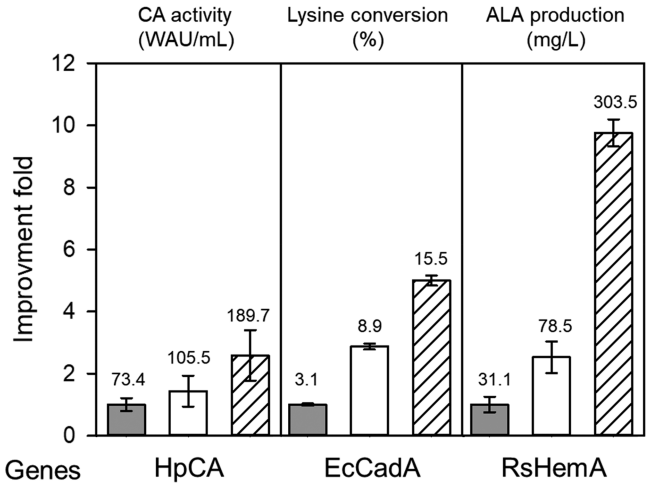

Figure 6. All the functional genes were cloned into the J23114-drived high-copy PDT7 system. The bars represent the increasing fold between DH5α wild type (gray bar) and DH5α harboring the basic cassette (white bar) or PDT7-harboring DH5α (lined bar). The number shown on the top of bars indicates the activity of CA (WAU), lysine conversion (%), and 5-ALA production (mg/L) for HpCA, EcCadA, and RsHemA, respectively. Error bars represent the standard deviation from three independent experiments (n = 3).

detected in wild-type DH5α was due to the native carbonic anhydrase expression.[27] The activity shown here is high enough for practical application in carbon fixation via the calcium carbonate precipitation.[28] The second functional protein was lysine decarboxylase catalyzing the decarboxylation of lysine to the diaminopentene (DAP) (Figure S7B), which is an important precursor for polymer production. We carried out the *in vitro* system for the transformation of lysine to DAP. After introducing extra CadA expression in our PDT7 system, it showed a 1.74-fold increased lysine conversion rate from 8.9% to 15.5% at a reaction time of 4 h when compared to DH5α harboring the basic cassette (Figure 6, EcCadA). This demonstrated that *in vitro* DAP production could be achieved directly using the cloning strain. The third targeted chemical was aminolevulinic acid (5-ALA) because this chemical could be applied in cancer diagnosis and treatment.[29] We selected the aminolevulinic acid synthase from *Rhodobacter sphaeroides* (RsHemA), which catalyzes the condensation of succinyl-CoA and glycine to 5-ALA (Figure S7C) and is commonly used for 5-ALA production.[29] The results showed that the 5-ALA production was 303.5 mg/L and 3.87-fold higher than that in DH5α harboring the basic cassette (Figure 6, RsHemA), although the yield is still lower than that reported in other literature,[30] which is attributed to insufficient expression of exporter and no optimization of fermentation.[31] Strain DH5α showed the higher plasmid stability due to *rec*A deficient, and thus could be directly applied for production without any genetic manipulation. Zhang and his colleague also demonstrated that solving the plasmid instability by *rec*A deletion enhanced the 5-ALA production by 21.4%.[32]

Apply PDT7 System to Enhance the Sensitivity of Cell-Based Biosensors. Cell-based biosensing is an emerging technique for *de novo* detection[33] and high-throughput screening,[34] in which the sensitivity would dominate the effectiveness. Therefore, we applied PDT7 to the cell-based biosensor for sensing glucose as a common chemical, and copper ion which is possibly one kind of pollutant in industry by changing the promoter of the J-series to P_{PI} and P_{copA}, respectively (Table S4). For glucose sensing, the catabolic activator protein (CAP) would bind with the cyclic AMP (cAMP) to activate the binding ability to the PI promoter, thus the PI promoter is repressed without glucose. On the contrary, glucose would inhibit the cAMP production via inactivation of adenylate cyclase converting ATP toward cyclic AMP (cAMP), thus the PI promoter will be turned on with glucose (Figure 7A). The dose−response curves of glucose using the basic and improved cassettes were shown in Figure 7B and Table 2. The sensing sensitivity was increased from 946.7 au/mM glucose to 5376.8 au/mM glucose, in terms of 27.34-fold increase on the sensitivity. On the other hand, copper ion sensing is controlled by CueR, a transcriptional activator binding with the copper ion to activate the copA promoter as shown in Figure 7C. The sensitivity of copper ion also showed an enhancement of 5.23-fold (Figure 7D and Table 2). A tightly regulated T7RNAP in the genome to enhance the sensitivity of small molecules biosensing has been already demonstrated.[35,36] Beyond integrating T7RNAP into the genome, limited work has focused on PDT7 with splitting T7RANP as a biosensing system.[20−22] Shis and his colleague showed that splitting T7RANP as a biosensor extended the operational range but decreased the dynamic range compared to full-length T7RNAP.[14] As the aim of the cell-based biosensor is sensitive detection of small molecules, full length T7RNAP would be a better choice. Here, we successfully demonstrated two kinds of promoter with enhanced sensitivity via the use of PDT7.

METHODS

Strains and Medium. All the strains, plasmids, and primers used in this study are listed in Table S5. For general cultivation, *E. coli* DH5α is cultured in LB medium (1.5% tryptone, 1.5% NaCl, and 0.5% yeast extract). Each construct was performed in *E. coli* DH5α and characterized in LB medium or MM9 medium (12.8 g/L Na_2HPO_4, 3 g/L KH_2PO_4, 0.5 g/L NaCl, 1 g/L NH_4Cl, 0.24 g/L $MgSO_4$, and 0.011 g/L $CaCl_2$) or MM9G (12.8 g/L Na_2HPO_4, 3 g/L KH_2PO_4, 0.5 g/L NaCl, 1 g/L NH_4Cl, 0.24 g/L $MgSO_4$, 0.011 g/L $CaCl_2$, and 4 g/L glucose) with 25 mg/L chloramphenicol if needed at 37 °C with shaking at 200 rpm. For ALA production, the medium was ALA_M9 containing 16 g/L $(NH_4)_2SO_4$, 16 g/L $Na_2HPO_4{\cdot}12H_2O$, 3 g/L KH_2PO_4, 2 g/L yeast extract, 1 g/L $MgSO_4{\cdot}7H_2O$, 0.01 g/L $MnSO_4{\cdot}7H_2O$, and 20 g/L glucose supplanted with 3 g/L glycine and 1 g/L succinate at the proper time.[31]

Plasmid Constructions. A traditional RE-based cloning method was applied. All restriction enzymes were purchased from New England Biolab. pSU-P_{LacI}-sfGFP and pSA-P_{LacI}-sfGFP were used as the initial cloning backbone (Figure S2A and S2B). Construction flow is shown in Figure S2C. Briefly, to construct the basic circuit, the promoter was replaced into

https://dx.doi.org/10.1021/acssynbio.9b00466
ACS Synth. Biol. 2020, 9, 613−622

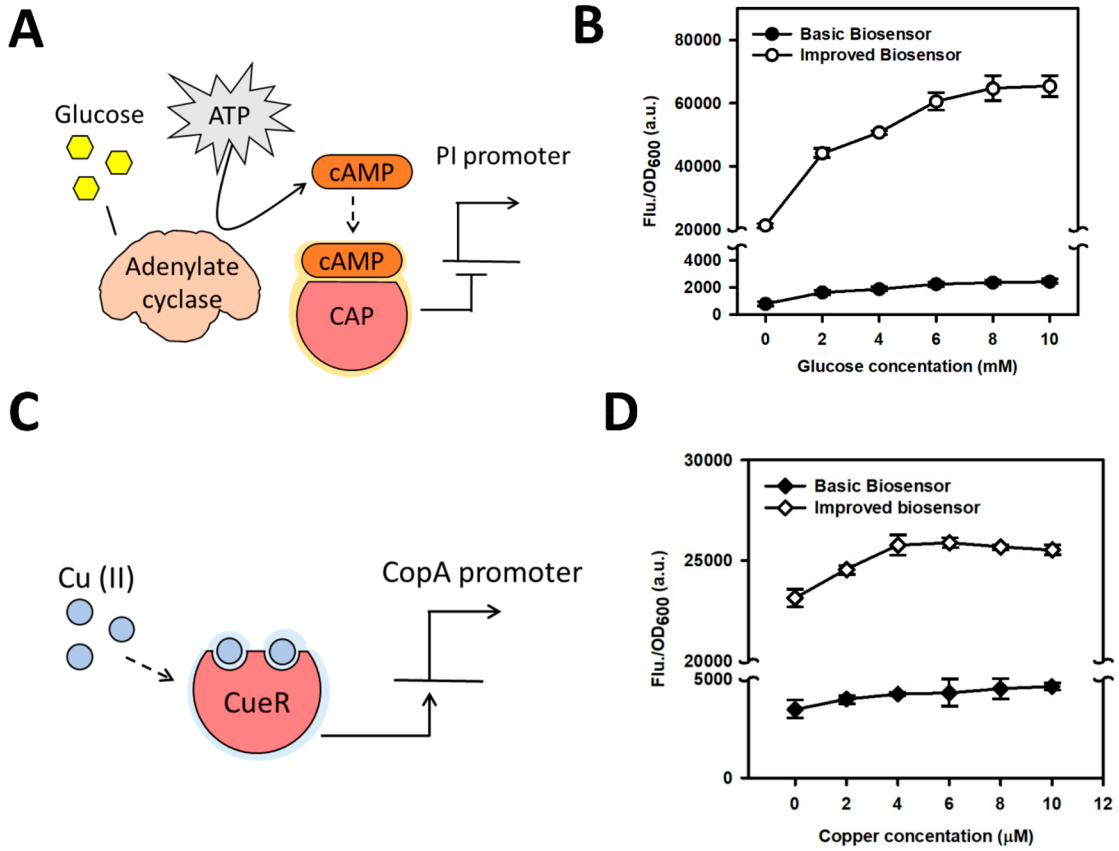

Figure 7. Application of PDT7 on the cell-based biosensor as an amplifier: (A) sensing mechanism of PI promoter; (B) dose−response curve of PI promoter in basic and improved genetic circuits; (C) sensing mechanism of copA promoter; (D) dose−response curve of copA promoter in basic and improved genetic circuits. Error bars represent the s.d. (standard deviation) of three independent experiments (n = 3).

Table 2. Application of PDT7 System in Whole Cell Sensing of Glucose and Copper Ion

sensing molecule	basic or improved	basal expression of sfGFP (a.u.)	sensitivity under linear region (a.u./conc.)	sensitivity increasing fold	linear region[a]
glucose	basic	946.7	196.9	27.34	0−8 mM
	improved	25967	5376.8		0−8 mM
copper ion	basic	3581.2	121.1	5.23	0−10 μM
	improved	23183	657.0		0−4 μM

[a]Linear region was determined by adjusting the R square value to near 0.95.

the location of the LacI promoter by digestion of *Xba*I and *Bam*HI. For the copA promoter it is amplified from the *E. coli* MG1655 colony by Ex-Taq (Takara, Japan). For the constitutive promoter and PI promoter, two complementary primers were first phosphorylated by T4 PNK (New England Biolab, UK) and then annealed to form the overhang of *Xba*I and *Bam*HI. After the construction of basic circuits, the sfGFP gene was replaced by T7RNA polymerase by digestion of *Hind*III and *Spe*I. The T7RNAP was amplified from the biobrick BBa_K145005. To construct the improved circuits, T7 promoter-driven sfGFP basic circuits were constructed using the method mentioned above. Finally, the improved circuits were constructed by the biobrick assembly method using T7 RNAP containing plasmid as a vector and T7P-driven sfGFP as an insert. For construction of different proteins in the J23114-driven high-copy PDT7 system, HpCA, EcCadA, and RsHemA were amplified and cloned into the pSU-J23114-PDT7 by *Bam*HI and *Pst*I.

Fluorescence Intensity and Biomass Measurement. A total of 200 μL of bacteria were taken into the 96-well plate with a transparent bottom and black wall. The biomass was determined by the optical density at 600 nm and the intensity of sfGFP was measured by excitation at 480 nm and emission at 510 nm using SpectraMax M2Microplate Readers (Molecular Devices, Sunnyvale, CA). For data processing, all the data of OD_{600} and fluorescence intensity were subtracted from the background value of the LB medium.

Determination of Plasmid Copy Number (PCN). Bacterial cells were collected by centrifugation and washed twice with deionized water. Afterward, the cells were resuspended in deionized water and then incubated at 95 °C for 10 min.[37] By centrifugation, the supernatant was applied for qPCR using the EvaGreen qPCR System-ROX I (GeneDireX, Germany) and StepOnePlus Real-Time PCR System (Applied Biosystems, USA). In the *E. coli* system, sfGFP was used as the targeted gene for evaluation of PCN, and one copy gene, GroES, was selected as the reference gene.

qRT-PCR. The relative transcription of genes was evaluated by qRT-PCR using the StepOnePlus Real-Time PCR System (Applied Biosystems, USA). Total RNA was extracted using the Total RNA Isolation Kit (Blood/Cultured Cell/Fungus) (GeneDireX, Germany). cDNA was produced using the

https://dx.doi.org/10.1021/acssynbio.9b00466
ACS Synth. Biol. 2020, 9, 613−622

SuperScript III First-Strand Synthesis System (Invitrogen USA). The concentration of cDNA was measured by the nano2000 system. A 200 ng sampling of cDNA was subjected to qRT-PCR using EvaGreen qPCR System-ROX I (GeneDireX, Germany). The 16S gene was selected as the endogenous gene to calculate the relative mRNA expression by the $2^{-\Delta\Delta C_{T.}}$

SDS-PAGE. The cells were harvested and then washed twice with deionized water. The cell density was adjusted to an OD_{600} of 10 as the sample. Afterward, the sample was analyzed by SDS-PAGE, which contained 12% separating gel and 4% stacking gel. Proteins were visualized by staining with Coomassie blue R-250 and were scanned by the image scanner (Biolab2000, Taiwan).

Enzyme Assay for Carbonic Anhydrase (CA). The cell harboring the pSU-J23114-PDT7-HpCA* was precultured first and then cultured in LB supplemented with 25 mg/L chloramphenicol for 12 h. Afterword, the cell was collected, washed three times by deionized water and finally adjusted to OD_{600} at 5 for further use. The activity assay of carbonic anhydrase was conducted as in our previous publication. Briefly, 9 mL of ice-cold Tris-HCl (20 mM, pH 8.3) buffer and 0.2 mL of enzyme were mixed and put in a 20 mL sample bottle at 0 °C under stirring. Then, 6 mL of ice-cold CO_2-saturated solution was added into the sample bottle immediately.[38] The time in seconds over which the pH value dropped from 8.3 to 6.3 was recorded. The CA activity was calculated by a Wilbur−Anderson unit (WAU) per milliliter of sample. The definition for WAU is $(T_0 - T)/T$, which T_0 and T are the time from pH 8.3 to 6.3 without and with CA.

Characterization of Lysine Decarboxylase (CadA). The cell harboring the pSU-J23114-PDT7-EcCadA* was also preculturied and then culturied in LB for 12 h. The cell pellet was collected and washed three times with deionized water. Finally, the cell pellet was resuspended in reaction buffer (146 g/L L-lysine monohydrochloride and 0.05 mM pyridoxal phosphate in a 0.9% NaCl solution) to reach OD_{600} at 4. The reaction system was held at 37 °C with 200 rpm shaking for 4 h. The lysine was quantified by ninhydrin assay. The 330 μL solution I (25 g/L in $FeCl_3$ in absolute ethanol), 185 μL solution II (10 g/L Ninhydrin in 0.1 M citrate pH2.0) and 10 μL sample were mixed and incubated in 100 °C for 30 min.[39] The mixture was centrifuged, and the supernatant fragment was measure using a spectrophotometer at the wavelength of 480 nm (SpectraMax 340, Molecular Devices, USA).

5-ALA Production and Quantification. A preculture was performed on the colony harboring pSU-J23114-PDT7-RsHemA*, and then the precultural cell was inoculated in 50 mL of MM9 medium. The precursor of 3 g/L glycine and 1 g/L succinate to produce ALA was added when the cell density of OD_{600} reached to 0.8, and the cells were harvested at 24 h. For analysis of 5-ALA production, Ehrlich's reagent[40] was used. A 500 μL aliquot of the sample or standard solution was well mixed with 500 μL of 1 M acetate buffer (pH 4.6) and 100 mL of acetylacetone. Subsequently, the mixture was heated at 100 °C for 10 min. After the mixture was cooled to room temperature, 100 μL was mixed with 100 μL of freshly prepared modified Ehrlich's reagent (0.1 g/mL *p*-dimethylaminobenzaldehyde (DMAB) and 0.16 mL/mL hypochlorous acid in glacial acetic acid in 96-well plates under minimal lighting. Lastly, the absorbance at 553 nm was measured with a spectrophotometer after 10 min (SpectraMax 340, Molecular Devices, USA).

Dose−Response Curve. Bacteria were precultured in LB medium for 12 h. A 1% (v/v) broth was inoculated into 3 mL of fresh LB medium and MM9 medium with different concentrations of copper ion and glucose, respectively, for copA promoter and PI promoter. The biomass and fluorescent intensity were measured at 12 h as mentioned above.

Data Analysis. The dose−response curve was modeled by the linear equation as follows.

$$y = y_0 + mx$$

The meaning of y and y_0 was mentioned above. Here, m represents the change in specific fluorescence intensity per unit concentration of targeted analytes. The linear region was determined by switching the targeted range and maintaining the R square value higher than 0.95. These parameters (i.e., b, y_0, and m) can be estimated by fitting the experimental data with SigmaPlot 12.1 software (Systat Software, USA) according to the manufacturer's instructions. Linear least-squares regression was used to minimize the error between the fitted and actual data.

■ ASSOCIATED CONTENT

Supporting Information

The Supporting Information is available free of charge on the ACS Publications Web site. The Supporting Information is available free of charge at https://pubs.acs.org/doi/10.1021/acssynbio.9b00466.

(PDF)

■ AUTHOR INFORMATION

Corresponding Author

I-Son Ng − *Department of Chemical Engineering, National Cheng Kung University, Tainan 70101, Taiwan;* orcid.org/0000-0003-1659-5814; Phone: +866-62757575; Email: yswu@mail.ncku.edu.tw; Fax: +86-62344496

Author

Shih-I Tan − *Department of Chemical Engineering, National Cheng Kung University, Tainan 70101, Taiwan;* orcid.org/0000-0002-7632-9991

Complete contact information is available at: https://pubs.acs.org/10.1021/acssynbio.9b00466

Author Contributions

S.I.T. and I.S.N. conceived of the study. S.I.T. performed all the experiments and original draft investigation. I.S.N. did methodology validation, supervised the experiments, and prepared, reviewed, and edited the manuscript.

Notes

The authors declare no competing financial interest.

■ ACKNOWLEDGMENTS

The authors are grateful to the financial support for this study provided by the Ministry of Science and Technology (MOST 108-2621-M-006-015, MOST 108-2221-E-006-004-MY3, and MOST 108-2218-E-006-006) in Taiwan.

■ REFERENCES

(1) Nielsen, A. A., Segall-Shapiro, T. H., and Voigt, C. A. (2013) Advances in genetic circuit design: novel biochemistries, deep part mining, and precision gene expression. *Curr. Opin. Chem. Biol.* 17 (6), 878−892.

(2) Siuti, P., Yazbek, J., and Lu, T. K. (2013) Synthetic circuits integrating logic and memory in living cells. *Nat. Biotechnol. 31* (5), 448−452.
(3) Tang, Q., Lu, T., and Liu, S. J. (2018) Developing a synthetic biology toolkit for *Comamonas testosteroni,* an emerging cellular chassis for bioremediation. *ACS Synth. Biol. 7* (7), 1753−1762.
(4) Zeldes, B. M. (2015) Extremely thermophilic microorganisms as metabolic engineering platforms for production of fuels and industrial chemicals. *Front. Microbiol. 6*, 1209.
(5) Chamberlin, M., Mcgrath, J., and Waskell, L. (1970) New RNA polymerase from *Escherichia coli* infected with bacteriophage T7. *Nature 228* (5268), 227−231.
(6) Studier, F. W., and Moffatt, B. A. (1986) Use of bacteriophage T7 RNA polymerase to direct selective high-level expression of cloned genes. *J. Mol. Biol. 189* (1), 113−130.
(7) Davanloo, P., Rosenberg, A. H., Dunn, J. J., and Studier, F. W. (1984) Cloning and expression of the gene for bacteriophage T7 RNA polymerase. *Proc. Natl. Acad. Sci. U. S. A. 81* (7), 2035−2039.
(8) Sousa, R., Chung, Y. J., Rose, J. P., and Wang, B. C. (1993) Crystal structure of bacteriophage T7 RNA polymerase at 3.3 Å resolution. *Nature 364* (6438), 593−599.
(9) Cheetham, G. M., and Steitz, T. A. (1999) Structure of a transcribing T7 RNA polymerase initiation complex. *Science 286* (5448), 2305−2309.
(10) Jia, Y., and Patel, S. S. (1997) Kinetic mechanism of transcription initiation by bacteriophage T7 RNA polymerase. *Biochemistry 36* (14), 4223−4232.
(11) Temiakov, D., et al. (2000) The specificity loop of T7 RNA polymerase interacts first with the promoter and then with the elongating transcript, suggesting a mechanism for promoter clearance. *Proc. Natl. Acad. Sci. U. S. A. 97* (26), 14109−14114.
(12) Wang, W., et al. (2018) Bacteriophage T7 transcription system: an enabling tool in synthetic biology. *Biotechnol. Adv. 36* (8), 2129−2137.
(13) Temme, K., Hill, R., Segall-Shapiro, T. H., Moser, F., and Voigt, C. A. (2012) Modular control of multiple pathways using engineered orthogonal T7 polymerases. *Nucleic Acids Res. 40* (17), 8773−8781.
(14) Shis, D. L., and Bennett, M. R. (2013) Library of synthetic transcriptional AND gates built with split T7 RNA polymerase mutants. *Proc. Natl. Acad. Sci. U. S. A. 110* (13), 5028−5033.
(15) Segall-Shapiro, T. H., Meyer, A. J., Ellington, A. D., Sontag, E. D., and Voigt, C. A. (2014) A 'resource allocator' for transcription based on a highly fragmented T7 RNA polymerase. *Mol. Syst. Biol. 10* (7), 742.
(16) Meyer, A. J., Ellefson, J. W., and Ellington, A. D. (2015) Directed evolution of a panel of orthogonal T7 RNA polymerase variants for in vivo or in vitro synthetic circuitry. *ACS Synth. Biol. 4* (10), 1070−1076.
(17) Kushwaha, M., and Salis, H. M. (2015) A portable expression resource for engineering cross-species genetic circuits and pathways. *Nat. Commun. 6* (1), 7832.
(18) Liang, X., Li, C., Wang, W., and Li, Q. (2018) Integrating T7 RNA polymerase and its cognate transcriptional units for a host-independent and stable expression system in single plasmid. *ACS Synth. Biol. 7* (5), 1424−1435.
(19) Shis, D. L., and Bennett, M. R. (2013) Library of synthetic transcriptional AND gates built with split T7 RNA polymerase mutants. *Proc. Natl. Acad. Sci. U. S. A. 110* (3), 5028−5033.
(20) Han, T., Chen, Q., and Liu, H. (2017) Engineered photoactivatable genetic switches based on the bacterium phage T7 RNA polymerase. *ACS Synth. Biol. 6* (2), 357−366.
(21) Baumschlager, A., Aoki, S. K., and Khammash, M. (2017) Dynamic blue light-inducible T7 RNA polymerases (Opto-T7RNAPs) for precise spatiotemporal gene expression control. *ACS Synth. Biol. 6* (11), 2157−2167.
(22) Pu, J., Zinkus-Boltz, J., and Dickinson, B. C. (2017) Evolution of a split RNA polymerase as a versatile biosensor platform. *Nat. Chem. Biol. 13* (4), 432−438.
(23) Zhang, J., Kang, Z., Chen, J., and Du, G. (2015) Optimization of the heme biosynthesis pathway for the production of 5-aminolevulinic acid in *Escherichia coli*. *Sci. Rep. 5* (1), 8584.
(24) Zhao, H., Zhang, H. M., Chen, X., Li, T., Wu, Q., Ouyang, Q., and Chen, G. Q. (2017) Novel T7-like expression systems used for *Halomonas*. *Metab. Eng. 39*, 128−140.
(25) Kang, C. W., et al. (2018) Synthetic auxotrophs for stable and tunable maintenance of plasmid copy number. *Metab. Eng. 48*, 121−128.
(26) Tyo, K. E., Ajikumar, P. K., and Stephanopoulos, G. (2009) Stabilized gene duplication enables long-term selection-free heterologous pathway expression. *Nat. Biotechnol. 27* (8), 760−765.
(27) Hsu, K. P., Tan, S. I., Chiu, C. Y., Chang, Y. K., and Ng, I. S. (2019) ARduino-pH Tracker and screening platform for characterization of recombinant carbonic anhydrase in *Escherichia coli*. *Biotechnol. Prog. 35*, e2834.
(28) Tan, S. I., et al. (2018) Efficient carbon dioxide sequestration by using recombinant carbonic anhydrase. *Process Biochem. 73*, 38−46.
(29) Takahashi, T., et al. (2016) The clinical trial for photodynamic diagnosis mediated 5-ALA for peritoneal metastasis due to advanced gastric cancer. *J. Clin. Oncol. 34* (4), 71.
(30) Kang, Z., Ding, W., Gong, X., Liu, Q., Du, G., and Chen, J. (2017) Recent advances in production of 5-aminolevulinic acid using biological strategies. *World J. Microbiol. Biotechnol. 33* (11), 200.
(31) Kang, Z., Wang, Y., Gu, P., Wang, Q., and Qi, Q. (2011) Engineering *Escherichia coli* for efficient production of 5-aminolevulinic acid from glucose. *Metab. Eng. 13* (5), 492−498.
(32) Zhang, J., Weng, H., Zhou, Z., Du, G., and Kang, Z. (2019) Engineering of multiple modular pathways for high-yield production of 5-aminolevulinic acid in *Escherichia coli*. *Bioresour. Technol. 274*, 353−360.
(33) Slomovic, S., Pardee, K., and Collins, J. J. (2015) Synthetic biology devices for in vitro and in vivo diagnostics. *Proc. Natl. Acad. Sci. U. S. A. 112* (47), 14429−14435.
(34) Lim, H. G., Jang, S., Jang, S., Seo, S. W., and Jung, G. Y. (2018) Design and optimization of genetically encoded biosensors for high-throughput screening of chemicals. *Curr. Opin. Biotechnol. 54*, 18−25.
(35) Kim, S. K., et al. (2018) A genetically encoded biosensor for monitoring isoprene production in engineered *Escherichia coli*. *ACS Synth. Biol. 7* (10), 2379−2390.
(36) Kim, H. J., et al. (2016) Development of a highly specific and sensitive cadmium and lead microbial biosensor using synthetic CadC-T7 genetic circuitry. *Biosens. Bioelectron. 79*, 701−708.
(37) Segall-Shapiro, T. H., Sontag, E. D., and Voigt, C. A. (2018) Engineered promoters enable constant gene expression at any copy number in bacteria. *Nat. Biotechnol. 36* (4), 352−358.
(38) Wilbur, K. M., and Anderson, N. G. (1948) Electrometric and colorimetric determination of carbonic anhydrase. *J. Biol. Chem. 176* (1), 147−154.
(39) Friedman, M. (2004) Applications of the ninhydrin reaction for analysis of amino acids, peptides, and proteins to agricultural and biomedical sciences. *J. Agric. Food Chem. 52* (3), 385−406.
(40) Manzerall, D., and Granick, S. (1956) The occurrence and determination of delta aminolevulinic acid and porphobilinogen in urine. *J. Biol. Chem. 219* (1), 435−436.

https://dx.doi.org/10.1021/acssynbio.9b00466
ACS Synth. Biol. 2020, 9, 613−622